oceans

MDPI

Article

Strong Effects of Sun Exposure on Oyster Shell Corrosion and Compensatory Calcification: A Factor Confounding Coastal Acidification Responses

David J. Marshall [1,*,‡], Natasha Khairul [1,‡], Naziratul Syaziyah Yahya [1], Norazimah Duraman [2] and James R. Jennings [2]

[1] Environmental and Life Sciences, Faculty of Science, Universiti Brunei Darussalam, Gadong, Bandar Seri Begawan BE1410, Brunei; natashakhairul1542@gmail.com (N.K.); naziratulsyaziyah@gmail.com (N.S.Y.)
[2] Applied Physics, Faculty of Science, Universiti Brunei Darussalam, Gadong, Bandar Seri Begawan BE1410, Brunei; norazimah.duraman@ubd.edu.bn (N.D.); james.jennings@ubd.edu.bn (J.R.J.)
* Correspondence: david.marshall@ubd.edu.bn
‡ These authors contributed equally to this work.

Abstract

The dynamics of calcium carbonate structures in marine organisms (skeletons and shells) has become increasingly important due to heightened interest in marine environmental acidification. Research into molluscan shell corrosion and calcification in response to acidification is typically carried out in laboratory-controlled settings, which often overlooks the intricate interactions found in natural environments. Mollusks inhabiting intertidal zones are especially susceptible to intense shell weathering caused by tidal cycles of heating, cooling, wetting, and drying, exacerbated by solar radiation during periods of air exposure. We investigated the effect of sun exposure (solar radiative heating) on both outer shell corrosion and inner shell compensatory calcification in the tropical oyster, *Saccostrea scyphophilla*. Shell properties were compared between oysters from neighboring populations in sun-exposed and shaded habitats. Habitat temperatures were measured using iButtons, and right shell valve corrosion was quantified. Compensatory calcification was assessed through measurements of shell thickness, shell density, shell compression strength, and mineralogical properties. Our results revealed that oysters in the sun that experience global irradiance, higher temperature peaks and broader daily temperature ranges (averaging an increase of 10 °C) show considerably greater outer shell surface corrosion (87%) compared to shaded oysters (31%) that experience only diffuse irradiance. Sun-exposed shells also become thickened in the midsection and around the adductor muscle, and they are slightly stronger, indicating compensation for the outer shell loss. These findings highlight the need for caution when interpreting molluscan shell dynamics based on laboratory marine acidification protocols that fail to account for the many natural environmental factors influencing shell formation and dissolution.

Keywords: bivalves; calcifiers; dissolution; molluscs; ocean acidification; oysters; temperature

Check for updates

Academic Editor: Beatriz Morales-Nin

Received: 9 January 2026
Revised: 31 March 2026
Accepted: 20 April 2026
Published: 6 May 2026

Copyright: © 2026 by the authors. Licensee MDPI, Basel, Switzerland. This article is an open access article distributed under the terms and conditions of the Creative Commons Attribution (CC BY) license.

1. Introduction

Many coastal marine environments become acidified through industrialization and urban development, and naturally through estuarine acidification (planktonic CO_2 elevation

and acidified groundwater infiltration) [1–6]. In recent years, investigation on marine environmental acidification has gained prominence due to the effect of elevated atmospheric CO_2 on the global ocean surface water, termed ocean acidification (QA) [7,8]. Changes in the ocean surface water chemistry, particularly an increase in H^{+1} and $HCO_3{}^{-1}$ ions and the reduction in $CO_3{}^{-2}$, can disrupt the normal capabilities of marine organisms, and the functioning of ecosystems [9,10]. Calcifying organisms that form shells or skeletons are especially impacted by a lowered calcification rate (laying down of the shell) and/or a greater rate of passive shell dissolution (loss of outer shell layer) [11–13]. Accordingly, molluscan shell thinning is commonly reported in laboratory-controlled experiments that simulate expected OA conditions by 2100 [14,15]. Thinner shells can impair locomotor activity and facilitate predation vulnerability through less robust outer shell protection, but also can reduce organismal fitness, potentially causing population decline and a change in ecosystem functioning [12,16,17]. However, laboratory protocols omit multiple interacting natural abiotic and biotic factors that alter shell calcification dynamics. For example, such protocols seldom account for shell weathering caused by wave action and highly variable temperature and salinity conditions that characterize tropical coastal and intertidal ecosystems. Furthermore, the effect of biotic interactive stressors on shell production, such as food source limitation, competition, and predation, are excluded or inappropriately considered in laboratory experiments [18–20]. Moreover, laboratory acidification studies are typically short-term, excluding lifelong responses of organisms to environmental change [21]. Field studies on organismal shell dynamics contribute to a better understanding of multifactorial interactions and provide opportunities to compare and validate laboratory responses to marine acidification [6,22,23].

In contrast to blue ocean ecosystems, coastal ecosystems experience highly variable abiotic conditions (temperature, salinity, turbidity, and pH) [1,4,12,24–26]. Air exposure is a primary environmental stressor in intertidal ecosystems, during which organisms experience direct solar radiation, which usually accelerates heating and drying between periods of cooling and wetting during tidal immersion in seawater. These conditions promote physical weathering (or corrosion) of calcium carbonate shells, which operates in tandem with outer shell loss through dissolution, the chemical breakdown of the shell in acidified seawater. Intertidal mollusks have evolved mechanisms for countering these environmental forces and for preserving shell integrity, including forming a thicker outer organic periostracum, increasing the shell protein content, building a more compact shell, and shifting mineral composition toward the more resistant calcite relative to aragonite [27–36]. However, the mechanisms and capacities to resist shell corrosion and dissolution vary greatly among molluscan species [24,36,37]. The shells of oysters, among the most prevalent molluscan intertidal rocky shore inhabitants, are typically prone to corrosion, despite having high calcite content [37]. Oysters are more commonly observed on sun-exposed rock surfaces, and even though they sometimes inhabit shaded crevices and the undersurfaces of rocks, little is known about the influence of habitat on their shell dynamics. The Asian oyster, previously referred to as *Saccostrea mordax*, but recently confirmed as *S. scyphophilla*, forms extensive reefs along the Bruneian coastline, inhabiting both sun-exposed and shaded surfaces on natural and artificial rocky shores [38–40]. These circumstances facilitate the comparison of shell attributes between sun-exposed and juxtaposed shaded individual oysters, enabling the assessment of the effect of solar exposure, with all other natural environmental factors being equal.

Molluscan shells respond to environmental conditions in complex ways, which can be grouped simply into three categories: (1) external shell corrosion (including dissolution), (2) shell calcification at the growing edge, and (3) inner shell thickening [24,41–43]. Growth-related secondary inner shell calcification in older shell regions, originally laid down as

relatively thin layers to support the functioning of smaller individuals, is commonly overlooked in short-term, laboratory-based OA experiments. The capability to thicken any region of the shell is important for repair from injury (failed predation), as well as for ensuring the maintenance of size-appropriate shell thickness following external shell loss, including that caused by corrosion or dissolution (compensatory calcification) [24,35,42,43]. Many laboratory-controlled acidification studies measure shell thickness at the growing edge, which not only confounds simultaneous incipient dissolution and calcification but also excludes deeper compensatory shell production associated with lifetime shell maintenance [24,42]. On the other hand, field studies offer the opportunity to capture such lifetime responses [24].

This study aimed to assess the effects of sun exposure on shell dynamics of *Saccostrea scyphophilla*. Using a natural field experiment to compare between sun-exposed and shaded oysters, we determined (1) habitat temperature conditions, (2) the pattern and degree of shell corrosion, and (3) attributes of compensatory calcification, including shell thickness, shell density, shell strength, and the calcite–aragonite content. We hypothesized that sun exposure substantially influences the shell dynamics of intertidal mollusks, representing a confounding factor in interpretations of organismal responses to environmental acidification (shell dissolution).

2. Materials and Methods

2.1. Study Sites and Habitat Temperature

The study was conducted at two localities, a natural rocky shore at the Empire Beach and an artificial shore at Tungku Beach, Brunei. Two sites were selected at each locality, giving a total of four sites for both sun-exposed (global irradiance = direct and diffuse solar irradiance) and shaded microhabitats (diffuse irradiance only): site A, 4°58′06.4″ N 114°51′21.1″ E, site B, 4°58′07.6″ N 114°51′20.2″ E , site C, 4°58′13.2″ N 114°52′00.7″ E, and site D, 4°58′16.7″ N 114°51′53.8″ E (Figure 1). The sites were separated by several kilometers and the habitats were located less than a meter apart from one another.

Solar irradiance differs fundamentally between sunned and shaded habitats. Whereas sunned habitats experience global irradiance (both direct and diffuse irradiance), the shaded habitats experience only diffuse irradiance, which is about 10–20% of the global irradiance on a horizontal surface during midday in the tropics. Diffuse and direct sunlight also have a different spectral distribution of energy. Because UV is scattered more strongly than visible and infrared light (because it has a shorter wavelength), the shaded UV intensity is 40–60% of the unshaded intensity. A previous study of local rocky shore habitats has determined the average global solar irradiance of sun-exposed surfaces (1084.93 $W \cdot m^{-2}$, over a 2 h period near midday) and how this relates to habitat temperature (Te) [44]. In the present study we determined Te in the oyster habitats using temperature dataloggers (Thermochron iButtons, Analog Devices Inc., Wilmington, MA, USA). These loggers were glued to the rock surfaces adjacent to the oysters using silicon glue, and they were covered with white plastic bottle caps to prevent solar radiative heating of their metal surfaces. Temperature was recorded every 10 min for 13 days during both cooler and warmer seasons (November 2024 and May and June 2025; see Table S1). Daily temperature profiles were constructed (starting at 6h00), and maximum and minimum daily temperatures, as well as thermal ranges, were compared between the habitat types.

The South China Sea coastline of Brunei is allochthonously acidified through highly localized groundwater infiltration into beach and rocky pool ecosystems. This effect is significant during low tides when pools become isolated from the oceanic seawater [2,6,25,36,45]. *Saccostrea scyphophilla* reefs, however, occur higher in the tidal zone above the pools, and during tidal inundation, they experience only oceanic seawater of ambient pH (~8.3 units),

salinity (~33 psu), and calcium content (~350 ppm) [2,24,36]. The Ω_{cal} and Ω_{ara} values in local oceanic waterbodies are ~5.06 and ~3.37, respectively [46].

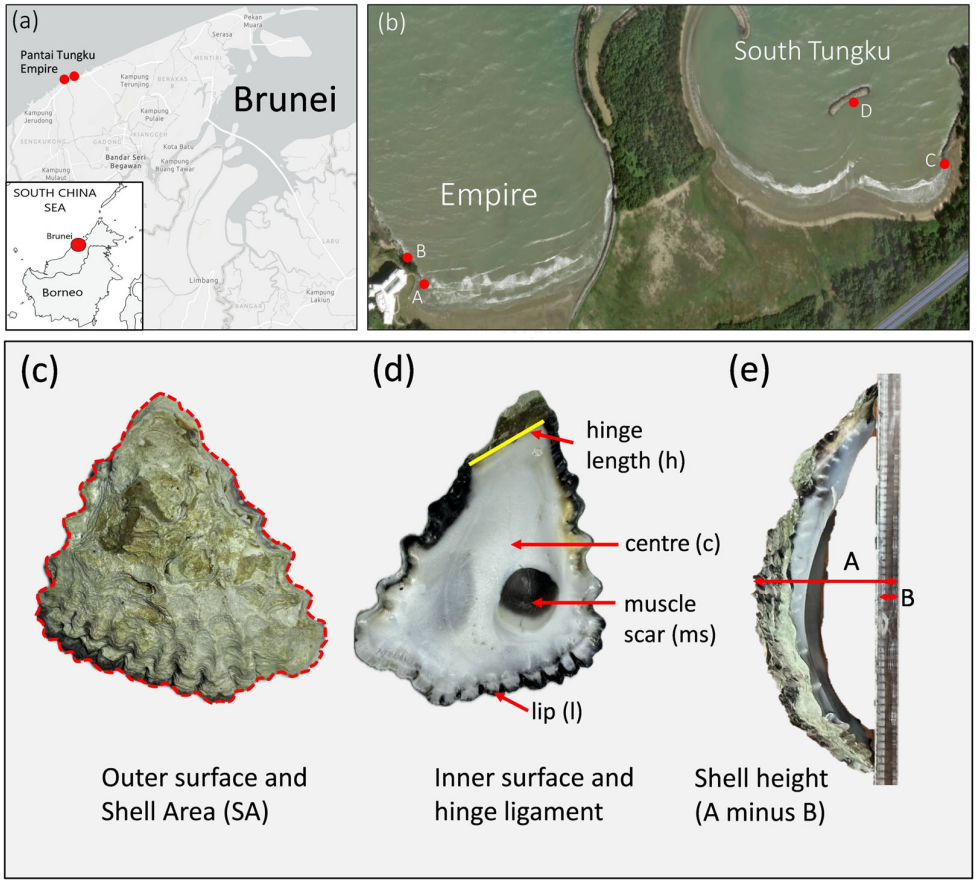


Figure 1. (**a**,**b**) Map and satellite image showing the locations of the sampling sites (marked A, B, C and D). (**c**) Outer surface of the right (upper) shell valve of a *Saccostrea scyphophilla* oyster. (**d**) Inner shell surface of an oyster showing the position of the hinge ligament (h) and muscle scar (ms). Shell thickness was measured at the center (c), muscle scar (ms), and shell lip (l). Shell height as an index of curvature was measured as in ((**e**) A is the height including surface plate and B is only the thickness of the surface plate).

2.2. Sampling and Shell Size

Twenty-five individual oysters were haphazardly collected from each of the eight site–habitat combinations, totaling 200 individual oysters. A genetic study has confirmed that all oysters were *Saccostrea scyphophilla* (Lee et al., in prep., Refs. [38,39]). The samples were returned to the laboratory and kept at −20 °C until further study. The oysters were later opened with a hammer and flathead screwdriver, and the right (upper) shell was removed for further examination. The shells were washed to remove surface debris, sediment, organic matter, and epibionts, and placed in an oven (Memmert UFE 500, Memmert GmbH & Co. KG, Schwabach, Germany) to dry at 70 °C for 24 h. The shells were then photographed on both sides, and measured using Olympus CenSens (Standard Version v4.3) digital software.

We intended to collect similar-sized shells to validate the shell corrosion results, as size relates to growth and age, and older shells are exposed to the environmental conditions for longer periods. Size was assessed using two measures, hinge length (h), a conservative estimate of growth, and total shell area (SA), a more dynamic estimate of growth (Figure 1). A Generalized Linear Model (GLM) for a normal distribution with a log-link function was used to compare the shell sizes across the habitat types (sun or shade).

All statistical analyses in this study were performed using Statistica Ver. 12 (StatSoft GmbH, Hamburg, Germany).

2.3. Shell Corrosion—Description, Quantification, and Reflectance

Based on shell surface corrosion patterns, including rib structure, transverse growth lamellae, and pigmentation (Figure 2), we distinguished three morphological types. These served as the basis for quantifying shell corrosion.

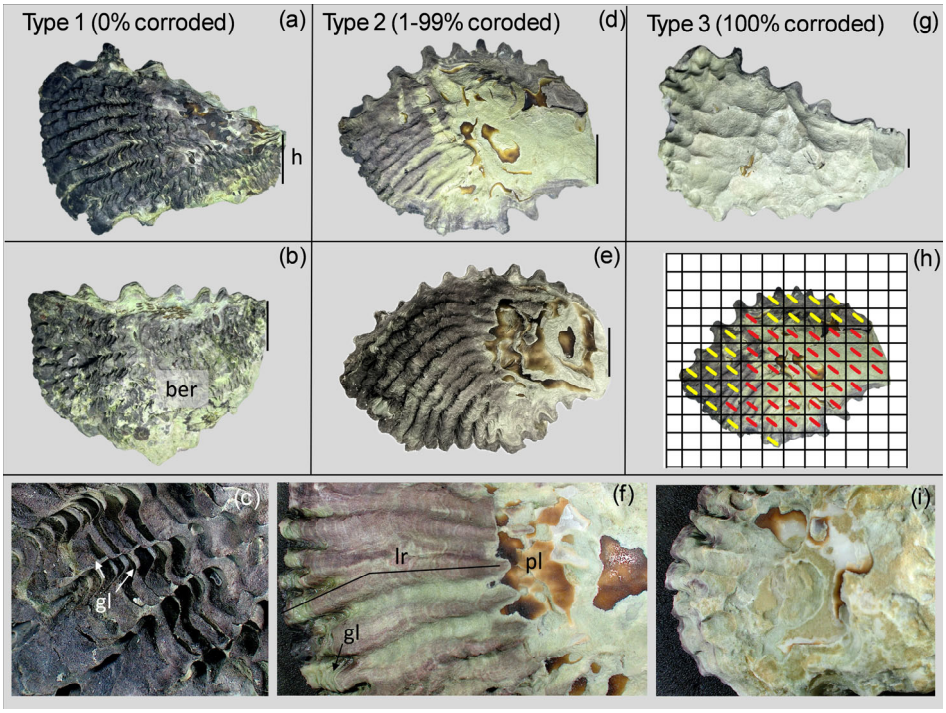


Figure 2. Oyster shell corrosion determination. Three levels (types) of corrosion were distinguished: (**a**–**c**) Type 1, 0% corrosion; (**d**–**f**) Type 2, 1–99% corrosion; and (**g**,**i**) Type 3 (100% corrosion. (**h**) A grid was placed over Type 2 images to determine the percentage of surface corrosion of Type 2 shells, which was determined from the count corroded cells, based on discolouration and texture (red marks = corroded cells, yellow marks = uncorroded cells). (**c**) Mid-shell of Type 1 showing well-structured growth lamellae (gl) and longitudinal ribs. (**f**) Type 2 shell showing the loss of growth lamellae (gl) and pigmented longitudinal ribs (lr) extending from the shell margin to the mid-shell region; more intensive corrosion in the mid-shell region exposes a brown proteinaceous (conchiolin) layer (pl). (**i**) Type 3 shell showing severe corrosion extending to the shell margin, and corroded longitudinal ribs and growth lamellae at the margin. h indicates hinge ligament in the oldest shell; ber, bioeroded mid-shell of Type 1. Higher magnifications at the growing shell margin and details of the conchiolin layer are shown in Figures A1 and A2.

- Type 1 shells show no corrosion (0%). They are darkly pigmented and characterized by clearly defined longitudinal ridges (or ribs) and structured growth lamellae extending from the shell margin to the hinge ligament (Figure 2a–c).
- Type 2 shells show variable corrosion (1–99%). They exhibit varying degrees of rib corrosion and pigmentation over the surface of the shell, though growth lamellae are usually not observed. A brown proteinaceous layer (conchiolin) is often exposed in the more heavily corroded older unpigmented shell region (Figures 2d–f, A1 and A2).
- Type 3 shells are completely corroded across the entire shell surface (100%), producing a light coloration. They have noticeable depressions, a complete loss of ribs, and growth lamellae, giving a smooth textured surface extending from the shell lip to the hinge ligament (Figures 2g,i, A1 and A2).

For Type 2 shells, the degree of shell corrosion was determined using a grid-based approach. Shell surface images were overlain with a grid of cells (12 × 15) using an online tool (https://www.photomultitool.com/grid, accessed on 17 February 2025; Figure 2h) and corrosion percentage was calculated as the number of corroded cells/total number of cells multiplied by 100. Corrosion, the loss of surface texture (lamellae and ridges), and pigmentation of a cell were scored in cases where the shell occupied >50% of the cell area, and corrosion occurred in over 50% of the cell (Figure 2h). The effects of site and habitat on shell corrosion, with site being a random effect, were tested using a General Linear Mixed Model (GLMM). The second analysis considering only the effect of habitat was based on a Kolmogorov–Smirnov test.

Diffuse reflectance spectra of the outer surfaces of sunned and shaded shells were recorded over the wavelength range of 185–1400 nm using a UV-Vis-NIR spectrophotometer equipped with an integrating sphere (Shimadzu UV-2600i (Shimadzu Corporation, Kyoto, Japan)). A disk of pressed barium sulfate powder was used as the reflectance standard. Three shells were selected from each habitat, and each shell was broken using a vice grip to obtain fragments of the upper (hinge) region, the middle (center) shell, and lower (lip), which were each measured separately. The shells were mounted by pressing against the input port (70 mm × 70 mm) of the integrating sphere with the outer surface facing inward.

2.4. Shell Thickness, Density, and Strength

We assessed compensatory internal shell production (calcification) from shell thickness, density, and strength. We determined shell thickness from a random sample of 20 shells from each habitat, representing Type 1 (0% corrosion) and Type 3 (100% corrosion) shells. Shell thickness was measured using a 0.001 mm precision digital micrometer at three shell regions—the lip, center, and muscle scar (Figure 1). The final recorded thickness was based on the average of three readings.

A compression strength test was performed on the same dry shells preciously used to determine thickness, as described above. The edges were gently sanded down to ensure good contact with the surface. Compression was applied at a loading speed of 3 mm/min (LLOYD Instruments LS100plus Universal Testing machine (AMTEK, Bognor Regis, UK)). Each shell was positioned on the compression plate with its outer surface facing upward. The maximum breaking point was determined as the peak force (N) that broke the shell at the midpoint (middle of the shell). The data were corrected and analyzed using Nexygen software (v4.5.1 issue 3).

Density was assessed from the ratio of mass (g) to volume (ml) for the entire right shell valve. Volume was determined from the displacement of water in a finely graduated measuring cylinder into which the shell valve was placed. The shells were then dried at 60 °C for 2 h in an airblown incubator, and then cooled and weighed using a 0.001 g precision balance (Mettler, Oakland, CA, USA).

2.5. Shell Crystallization

To assess whether shell crystallization varied among sunned and shaded shells, X-ray diffraction (XRD) patterns obtained from powdered shells were analyzed to estimate the aragonite/calcite content, lattice parameters, and calcite crystallite size and microstrain. Three shells selected from each habitat type were broken up into three sections—upper (hinge area), middle (center), and lower (lip)—using a hammer. Each section was then ground into fine powder using an agate mortar and pestle until a uniform particle size was achieved. The XRD patterns of the powdered samples were measured with Cu Kα radiation using a benchtop X-ray diffractometer (Malvern PANalytical Aeris Research Edition, Worcestershire, UK), and the obtained patterns were analyzed through Rietveld

refinement using PANalytical HighScore Plus, version 5.2. Before refining the samples, a macrocrystalline silicon standard was measured under identical instrumental conditions to determine the instrumental contribution to peak broadening. The samples were modeled as mixtures of three crystalline phases: calcite, aragonite, and α-quartz (to model traces of sand in some samples). Structural models were taken from the Crystallography Open Database.

3. Results

3.1. Habitat Temperature

Sun-exposed oysters experienced much higher daily thermal maxima and greater temperature ranges than shaded oysters. Mean daily thermal maxima in the sun exceeded shaded temperatures by ~10 °C ($p < 0.025$; Figure 3a,b; Table 1). Although the average minimum habitat temperature (26.1 °C) in the shade was higher than that in the sun-exposed habitat, probably due to the more insular conditions in the shade, this was not significantly different ($p > 0.1$; Figure 3a,b; Table 1). The mean daily maximum temperature in the shade approximated the regional ambient air temperature as recorded in a Stevenson screen. The mean daily temperature range in the sunned habitat, driven by the thermal maxima (43.4 °C), also exceeded that in the shaded habit by ~10 °C ($p < 0.025$; Figure 3; Table 1). Temperature differences between the habitats were influenced by solar radiation during air exposure, with temperatures in both habitats stabilizing at ~30 °C during tidal immersion (Figure 3c). Daily solar heating was rapid (2.9 °C/h) causing sunned shells to quickly dry completely during tidal emersion, whereas shaded shells typically remained moist throughout the tidal air emersion period.

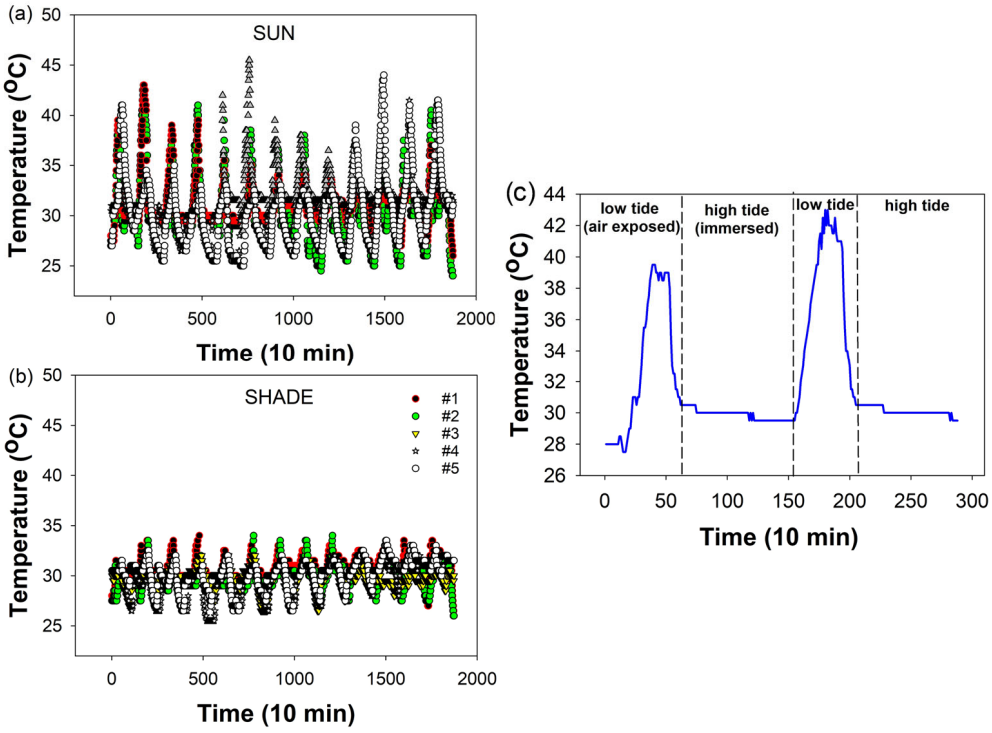


Figure 3. Field temperatures recorded in (**a**) sun-exposed and (**b**) shaded habitats over 13 days, starting and ending at 6h00. Five representative dataloggers for different sites are shown for each habitat type (see Table S1). (**c**) The first 2 days of recording for datalogger #2 sun, showing how temperature steeply rises due to solar radiation during air exposure and stabilizes at ~30 °C during seawater immersion. Minimum daily temperatures in the air typically fall below 30 °C in both habitats. Statistical comparisons are given in Table 1.

Table 1. Field temperature conditions in sun-exposed and shaded oyster habitats (NS, non-significant).

	Sun (Mean ± SD)	Shade (Mean ± SD)	Significance
Daily Max Temp	43.4 ± 1.5	33.5 ± 0.6	$p < 0.025$
Daily Min Temp	25.7 ± 1.3	26.1 ± 0.4	$p > 0.1$ (NS)
Daily Temp Range	17.7 ± 1.5	7.4 ± 0.5	$p < 0.025$

3.2. Shell Size and Corrosion

The shaded shells in the collection were slightly larger than the sun-exposed shells. Hinge lengths (mean ± SE) were, respectively, 13.09 ± 0.26 mm and 11.73 ± 0.26 mm (Wald Stat = 13.71; $p < 0.01$). Likewise, shell surface areas were 1192.12 ± 28.6 and 925.7 ± 28.4 mm^2 (Wald Stat = 47.6; $p < 0.01$). This suggests that the shaded shells were on average either older, assuming similar growth rates, or that they grew faster. With respect to shell corrosion, the sun-exposed shells were vastly more corroded (mean ± S.E = 87 ± 2.3% of the surface area) than the shaded shells (mean ± S.E = 31 ± 2.3%; $p < 0.001$; Kolmogorov–Smirnov; Figure 4a). The GLMM analysis, considering the effects of both site and habitat (sun or shade), showed that habitat had a strong effect (F = 236.6; $p < 0.001$), whereas the effect of site was invalidated in the model by non-homogeneity (Cohran C test; Figure 4b; Table 2). The overall result was strongly influenced by site D, which showed 0% median shell corrosion in shaded oysters (Figure 4b).

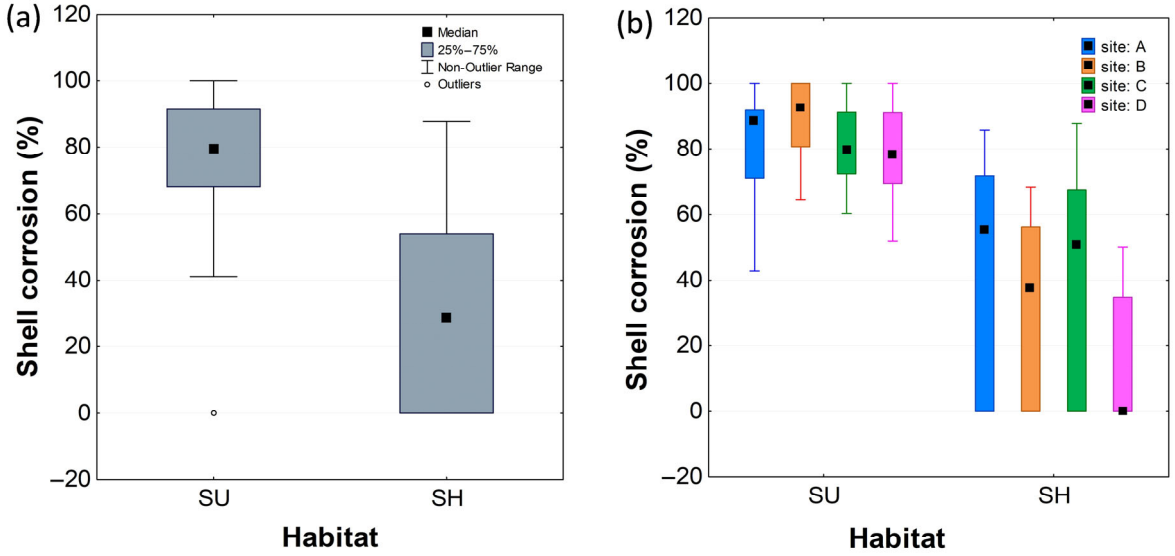


Figure 4. Effect of habitat and site on shell corrosion (median % surface area). (**a**) Habitat only and (**b**) habitat and site. SU, sun; SH, shade. Site locations are given in Figure 1.

Table 2. Effect of habitat and site on shell corrosion (General Linear Mixed Model).

Effect	Effect (F/R)	SS	Degr. of Freedom	MS	F	*p*
Intercept	Fixed	656,554.7	1	656,554.7	338.2	$p < 0.001$
Site	Random	5824.03	3	1941.3	3.6	$p = 0.015$
Habitat	Fixed	128,913.1	1	128,913.1	236.6	$p < 0.001$
Error		106,269.9	195	545.0		

3.3. Shell Reflectance

Consistent with their brighter visual appearance, the diffuse reflectance of sun-exposed shells is higher than that of shaded shells across the entire UV-visible-NIR spectral range (200–1400 nm; Figure S1). Both sun-exposed and shaded shells exhibit an absorption band (dip in reflectance) centered at 672–676 nm due to chlorophyll *a*, indicating the presence of biofilms comprising photosynthetic microorganisms at the surfaces of the shells. Multiple weak absorption bands at shorter wavelengths also arise from pigments contained in various microorganisms (e.g., diatoms, chlorophytes, cyanobacteria, and rhodophytes) [47,48]. At wavelengths where microbial pigments absorb strongly, the higher diffuse reflectance of sunned shells is consistent with a lower surface pigment density, implying reduced biomass and pigment content due to photoinhibition of microbial growth and photobleaching by solar radiation.

3.4. Shell Thickness, Density, and Strength

Shells located in the sun were thicker than shaded shells, with thickness varying across the shell surface (muscle scar, center, and lip). A factorial ANOVA using similar-sized snails (mean shell area sun = 1036 mm^2; shade = 1177 mm^2; $p > 0.10$, $n = 20$ for each habitat) showed that shell thickness varied relative to the habitat ($F = 15.19$, $p < 0.001$; Figure 5a; Table 3) and the position on the inner shell surface ($F = 51.68$, $p < 0.001$; Figure 5a; Table 3). The thickest shell in the samples was located at the attachment point of the adductor muscle in sun-exposed shells (mean thickness = 5.03 mm), and the thinnest shell was observed at the center in shaded shells (mean thickness = 2.75 mm; Figure 5a). While shell thickness at the muscle scar was greater than that at the center in both sunned and shaded shells, there was no significant difference in lip thickness between the habitats (Figure 5a). Compensatory calcification in sun-exposed shells was observed as a whiter shell deposit centrally and as a darker shell at the muscle scar (Figure 5b).

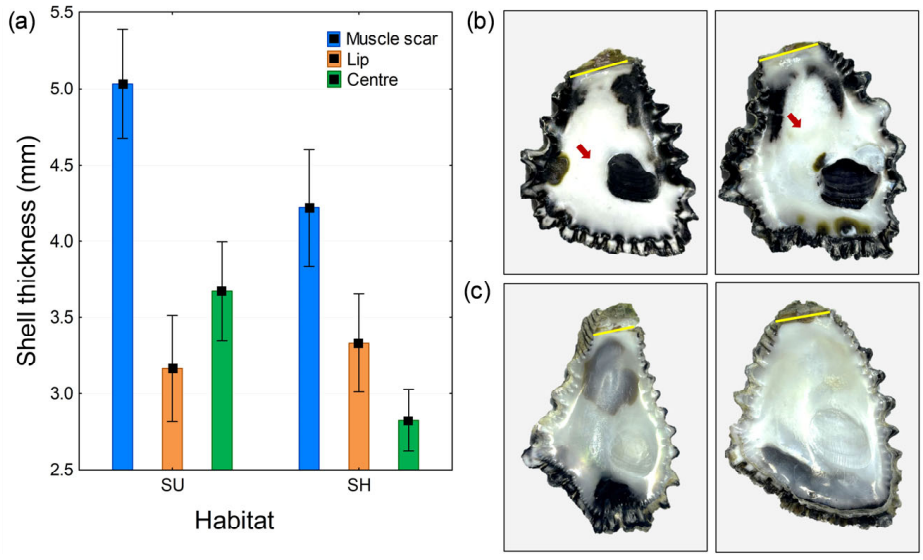


Figure 5. Shell compensatory calcification. (**a**) Effect of habitat and position on shell thickening (mean ± 95% CI); (**b**) inner surfaces of sun-exposed shells; and (**c**) shaded shells. Compensatory calcification in sun-exposed shells is observed as a brighter, whiter shell centrally (arrowed) and a darker shell at the muscle scar. The hinge ligament is indicated by the yellow line.

Table 3. Effects of habitat (sun, shade) and position (lip, center, and muscle scar) on shell thickening.

Effect	SS	Degr. of Freedom	MS	F	*p*
Habitat	7.4	1	7.4	15.2	$p < 0.001$
Shell	50.6	2	25.3	51.7	$p < 0.001$
Habitat × shell	6.6	2	3.3	6.8	$p < 0.01$
Error	55.8	114	0.5		

Shell density did not differ between shaded and sun-exposed oyster shells (mean ± SE, sun = 2.38 ± 0.05 g/mL; shade = 2.35 ± 0.05 g/mL; $F_{(1,38)} = 0.146$, $p = 0.704$; $n = 20$ for each habitat). However, shell strength (breaking point under applied compression) for similarly curved shells (shell height: mean sun = 10.4 mm; mean shade = 9.6 mm; $F_{(1,38)} = 1.9$; $p > 0.10$) was significantly greater in the sun-exposed shells (mean sun ± SE = 391.5 ± 32.4 N; mean shade = 216.5 ± 32.4 N; $p < 0.05$; $n = 20$ for each habitat, Kolmogorov–Smirnov Test). The combined observations for shell thickness, density, and strength suggest that the strengthening of sun-exposed shells derives from secondary thickening rather than shell density.

3.5. Shell Crystallization

Rietveld refinement of X-ray diffraction patterns of powdered shells (Figure S2) revealed no significant differences in average calcite/aragonite ratio, calcite crystallite size, and calcite out-of-plane (c-axis) lattice parameter *c* between sun-exposed and shaded shells. Small but significant differences in calcite microstrain (mean sun 0.078%; mean shade 0.098%; $p = 0.00076$; $n = 9$ for each habitat) and basal lattice parameter, *a* (mean sun 4.987 Å; mean shade 4.985 Å; $p = 0.032$; $n = 9$ for each habitat), were observed between habitat types. However, since the powdered samples represented a mixture of different shell microstructures (prismatic, foliated, and chalky layers), it was difficult to attribute these average crystallographic differences to specific biogenic features or to exclude the possibility that they arose from differential responses to grinding.

4. Discussion

Thermal conditions on tropical rocky shores are highly variable, fluctuating daily in response to changes in weather and cloud cover. Due to the lack of synchronization among dataloggers across different days, it was not possible to make direct comparisons of thermal regimes between sites. Additionally, the short duration of the recording period made it impractical to analyze seasonal or temporal differences. However, the data from Brunei weather stations indicated that monthly averaged daily maximum air temperatures are slightly lower (by approximately 2 °C) during the boreal winter months. Despite these limitations, grouping the collected data by habitat type revealed substantial differences in thermal regimes. The mean daily thermal maximum in sun-exposed habitats was 43.4 °C, whereas it was considerably lower at 33.5 °C in shaded habitats. Both habitat types exhibited a mean daily minimum temperature of ~25 °C (Figure 3 and Table 1). The daily thermal range in shaded habitats was ~7.4 °C, whereas it was ~17.7 °C in sun-exposed habitats. The highest maximum temperature recorded was 45.5 °C, which is notably lower than the upper temperatures experienced by *Echinolittorina* snails in the higher shore zone, which rise above 50 °C [49,50]. The daily maximum temperatures are determined by solar radiation during periods of air exposure, whereas relatively stable temperatures (~30 °C) are experienced during seawater submersion (Figure 3c). The temperature and tidal cycle differences among the habitats impart different rates of heating, cooling, wetting, and drying. Typically, oysters in shaded areas stay wet or moist during tidal emersion, whereas those in sun-exposed areas are more likely to dry out completely.

Although multiple factors, including seawater composition (salinity), pH conditions, turbidity, and sand scouring, may affect shell corrosion, these were considered to be similar across the study habitats, which otherwise varied greatly in solar exposure and thermal regime. The more extreme conditions of heating and drying caused enhanced outer shell corrosion in the sun-exposed oysters (Figure 2). Surface features of the right shell valves, such as growth lamellae and longitudinal ribs, were typically corroded away in sun-exposed oysters, which showed an average of 83% shell surface corrosion (compared to 31% in shaded oysters; Figures 2 and 4). Corrosion of sun-exposed shells occurred rapidly following the deposition of new pigmented and structured shell at the growing edge (Figure 2c,i); the sharp-edged growth lamellae observed in the shaded shells became rounded and were often completely worn down in sun-exposed shells (Figure A1). Unlike in other bivalves, the outer periostracum of oysters does not effectively protect the newly deposited shell against dissolution or corrosion [51]. In older shells, complete corrosion of the longitudinal ribs exposed proteinaceous conchiolin sheets, which have several functions, including resisting against predation [52]. These sheets later flaked off the shell surface (Figure A2a). Epibiotic and endolithic organisms (including sponge and algal microborers) also contribute to shell corrosion in ways that seem to differ across the habitat types. Shaded shells, which present more moderate conditions, were often modestly colonized by mussels, barnacles, and tubeworms (Figure A2b), whereas significant colonization of endolithic photosynthetic microbes was observed in corroded sun-exposed shells, especially at the interface of growth lamellae (Figures A1 and S1) [53]. During air exposure, boundary layer water that persists on the shaded oysters might become acidified through microbial respiration. There was, however, little evidence of greater shell dissolution in shaded compared to sun-exposed shells from which this boundary water layer was rapidly evaporated. Despite these various abiotic and biotic factors, solar exposure is demonstrated here to vastly override other influences of shell corrosion.

Direct absorption of solar radiation is expected to promote shell corrosion and erosion through several distinct mechanisms, all of which may be operating in parallel. The absorption of sunlight, especially ultraviolet (UV) light, by organic materials (e.g., conchiolin) in the shell will eventually lead to photochemical degradation, thereby accelerating the removal of the protective periostracum and the weakening the organic matrix that binds the calcite crystallites together near the growing lip. Light absorption by the organic matrix, as well as by surface biofilms that absorb strongly in the UV-visible-NIR (Figure S1; pristine calcite is an extremely weak absorber in the UV-visible-NIR spectral range), will also selectively heat the outer surface, leading to a thermal gradient between the outer, irradiated surface and the cooler, inner surface. Temperature gradients across any material, especially poor thermal conductors such as calcite, lead to thermal stresses that promote the formation of microcracks. Calcite is also known to exhibit anisotropic thermal expansion [52], so even in the absence of significant thermal gradients through the shell, thermal cycling will cause intergranular mismatch stresses, especially where differently oriented grains and thin organic interlayers restrict free thermal expansion. Regardless of the precise mechanisms, any thermally induced formation of microcracks in the calcite layer will increase the rate of mechanical erosion and chemical dissolution. Elevated shell surface temperatures will also directly promote calcite dissolution when wet because the dissolution rate of calcite increases with increasing temperature [54]. Finally, rapidly drying salt crystals under high temperature may enhance surface corrosion of sun-exposed shells, in contrast to the shaded shells, which remain damp at relatively low temperatures during tidal emersion.

The natural corrosion of sun-exposed shells in intertidal systems carries implications for predicting shell responses to ocean or coastal acidification (by 2100), as well as for the monitoring of these processes. Laboratory studies that assess acidification responses

that exclude the effect of solar radiation risk underestimating outer shell loss under natural circumstances (through corrosion and dissolution). Natural weathering should be accounted for in biomonitoring exercises where molluscan shells are used to indicate an organism's exposure to marine environmental acidification [2,6,22,25]. Using shell corrosion features, acidification biomonitoring (1) can capture an organism's lifelong exposure to temporally variable acidification (which could go undetected in a time-restricted recording period), (2) can enable large spatial scale assessment (rather than limited point localities where metering equipment is deployed), and (3) can allow for the investigation of shores subjected to powerful wave action (which prevent the deployment of sensitive metering equipment [2,6,22]). The present study, however, highlights the need for careful calibration of biomonitoring tools (shells), by use of control organisms that avoid solar exposure or experience limited acidification exposure.

Although mollusks have intrinsic shell repair capabilities and although shell thickness increases with shell growth, compensatory internal calcification in response to external shell loss is generally poorly considered in OA studies (but see [24,41,42,55,56]). Lifelong shell thickness compensation demonstrated on shell transections (from the apex to the shell margin) of *Nerita* snails from acidified intertidal settings is negated by short-term laboratory OA investigations [24]. Laboratory investigations often measure shell thickness at the growing margin of a mollusk, capturing primary shell growth, but also confounding simultaneous calcification and dissolution responses to acidified water exposure. The *Nerita* study shows that thinner shell at the lip under acidified field conditions, compared to non-acidified conditions, is readily compensated by internal calcification (shell deposition), such that overall shell thickness is similar among these different environmental circumstances [24]. We found no difference in oyster shell lip thickness (primary shell growth) between sun-exposed and shaded shells (Figure 5), which was expected as the oysters experience similar pH and substrate (HCO_3^{-1}, CO_3^{-2}, Ca^{+2}, Mg^{+2}) exposures in these different habitat types [24,46]. Significant shell thickening around the muscle scar and in the central shell region in sun-exposed oysters was associated with darker and lighter colored shell, respectively (Figure 5b,c). The thickening at the muscle attachment should be functionally significant considering that the greatest force is likely exerted at this point of the shell. This shell thickening may underlie the marginally greater strength observed in sun-exposed oysters. The sun-exposed shells also exhibited slightly lower microstrain and larger lattice parameter *a* than shaded shells. However, since the powdered samples represented a mixture of different shell microstructures (prismatic, foliated, and chalky layers), it was not possible to directly link these average crystallographic differences to the higher fracture strength of the sun-exposed shells. In summary, we showed that oysters compensate for external corrosive shell loss (weathering) under normal conditions of oceanic pH and carbonate concentrations through internal calcification, thereby maintaining shell strength crucial for functionality and ecological interactions.

5. Conclusions

Although shell dissolution is at the forefront of understanding organismal responses to OA, natural factors contributing to shell corrosion are poorly considered in laboratory studies. We show that solar radiation plays a significant role in physically corroding the shells of intertidal rocky shore oysters. We further show that oysters exhibit a compensatory response to corrosion-induced outer shell loss by building shell layers internally. The above circumstances and responses (e.g., shell repair) likely generalize across marine mollusks, with varying degrees of capability linked to differences in taxonomic background and life history traits. Such natural influences on molluscan shell dynamics need greater

consideration when interpreting laboratory (mesocosm) results and predicting organismal responses to OA and climate change.

Supplementary Materials: The following supporting information can be downloaded at: https://www.mdpi.com/article/10.3390/oceans7030039/s1, Figure S1: Diffuse reflectance spectra of the outer surfaces of sunned (red) and shaded (blue) oyster shells. Individual lines are based on fragments for different shells; Figure S2: Representative X-ray diffraction pattern of powdered oyster shell; Table S1: iButtons datalogger deployment.

Author Contributions: Conceptualization, D.J.M., N.D. and J.R.J.; methodology, D.J.M., N.K., N.S.Y., N.D. and J.R.J.; formal analysis, D.J.M. and J.R.J.; investigation, D.J.M., N.K., N.S.Y., N.D. and J.R.J.; data curation, N.K. and N.S.Y.; writing—original draft preparation, D.J.M. and N.K.; writing—review and editing, D.J.M., N.K., N.S.Y., N.D. and J.R.J.; supervision, D.J.M., N.D. and J.R.J.; project administration, D.J.M.; funding acquisition, D.J.M. All authors have read and agreed to the published version of the manuscript.

Funding: This research and the APC were funded by Universiti Brunei Darussalam, number UBD/RSCH/1.4/FICBF(b)/2021/033 and UBD/RSCH/1.4/FICBF/2025/004, awarded to D.M.

Data Availability Statement: The original contributions presented in this study are included in the article/Supplementary Materials. Further inquiries can be directed to the corresponding author.

Acknowledgments: No GenAI has been used for the purposes of generating text, data, or graphics, or for study design, data collection, analysis, or the interpretation of data.

Conflicts of Interest: The authors declare no conflicts of interest.

Appendix A

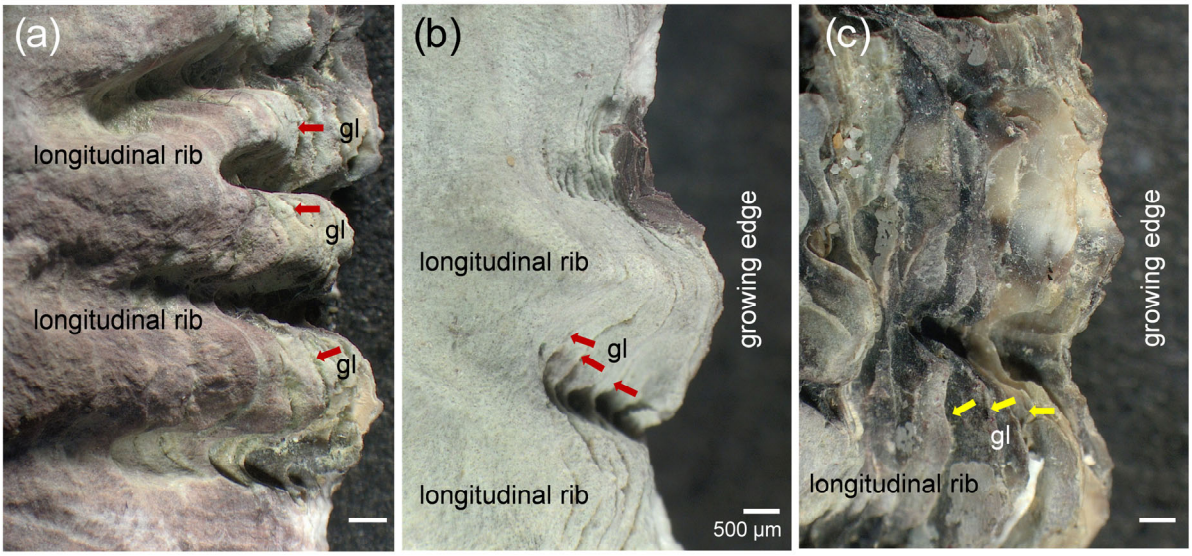


Figure A1. Outer surfaces of right shell valves of oysters at the growing edge. (**a**) Sun-exposed shell showing corroded growth lamellae (gl) and colonization by endolithic photosynthetic microorganisms (green color) between the lamellae. (**b**) Sun-exposed shell showing severe corrosion of recently formed lamellae. (**c**) Shaded shell showing sharp-edged growth lamellae projecting above the shell surface, which were sometimes broken off (see also Figure 2). Scale bars = 500 µm.

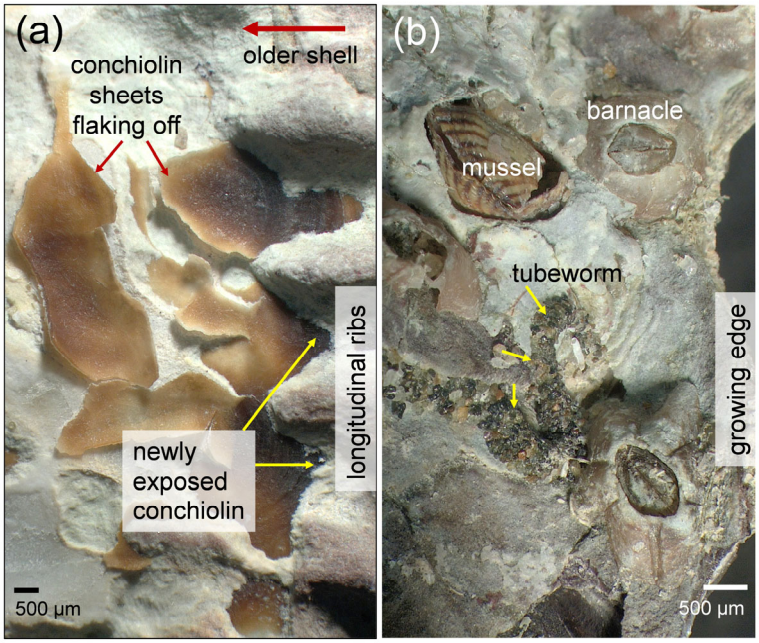


Figure A2. Outer surfaces of right shell valves of oysters. (**a**) Sun-exposed mid-shell region showing the initial exposure of conchiolin following the corrosion of the longitudinal ribs and the later flaking off of this proteinaceous layer. (**b**) Growing edge of a shaded shell showing mussel, barnacle, and tubeworm colonization.

References

1. Feely, R.A.; Alin, S.R.; Newton, J.; Sabine, C.; Warner, M.; Devol, A.; Krembs, C.; Maloy, C. The combined effects of ocean acidification, mixing, and respiration on pH and carbonate saturation in an urbanized estuary. *Estuar. Coast. Shelf Sci. J.* **2010**, *88*, 442–449. [CrossRef]
2. Marshall, D.J.; Santos, J.H.; Leung, K.M.Y.; Chak, W.H. Correlations between gastropod shell dissolution and water chemical properties in a tropical estuary. *Mar. Environ. Res.* **2008**, *66*, 422–429. [CrossRef] [PubMed]
3. Yao, H.; Wang, J.; Han, Y.; Jiang, X.; Chen, J. Decadal acidification in a subtropical coastal area under chronic eutrophication. *Environ. Pollut.* **2022**, *293*, 118487. [CrossRef]
4. Cai, W.-J.; Feely, R.A.; Testa, J.M.; Li, M.; Evans, W.; Alin, S.R.; Xu, Y.-Y.; Pelletier, G.; Ahmed, A.; Greeley, D.J.; et al. Natural and anthropogenic drivers of acidification in large estuaries. *Annu. Rev. Mar. Sci.* **2021**, *13*, 23–55. [CrossRef]
5. Harayashiki, C.A.Y.; Márquez, F.; Cariou, E.; Castro, Í.B. Mollusk shell alterations resulting from coastal contamination and other environmental factors. *Environ. Pollut.* **2020**, *265*, 114881. [CrossRef]
6. Marshall, D.J.; Abdelhady, A.A.; Wah, D.T.T.; Mustapha, N.; Gödeke, S.H.; DeSilva, L.C.; Hall-Spencer, J.M. Biomonitoring acidification using marine gastropods. *Sci. Total Environ.* **2019**, *692*, 833–843. [CrossRef]
7. Sabine, C.L.; Feely, R.A.; Gruber, N.; Key, R.M.; Lee, K.; Bullister, J.L.; Wanninkhof, R.; Wong, C.S.; Wallace, D.W.R.; Tilbrook, B.; et al. The oceanic sink for anthropogenic CO_2. *Science* **2004**, *305*, 367–371. [CrossRef]
8. Barrett, R.C.; Carter, B.R.; Fassbender, A.J.; Tilbrook, B.; Woosley, R.J.; Azetsu-Scott, K.; Feely, R.A.; Goyet, C.; Ishii, M.; Murata, A.; et al. Biological responses to ocean acidification are changing the global ocean carbon cycle. *Glob. Biogeochem. Cycles* **2025**, *39*, e2024GB008358. [CrossRef]
9. Nagelkerken, I.; Connell, S.D. Ocean acidification drives global reshuffling of ecological communities. *Glob. Change Biol.* **2022**, *28*, 7038–7048. [CrossRef]
10. Bednaršek, N.; Feely, R.A.; Pelletier, G.; Desmet, F. Global synthesis of the status and trends of ocean acidification impacts on shelled pteropods. *Oceanography* **2023**, *36*, 130–137. [CrossRef]
11. Duquette, A.; McClintock, J.B.; Amsler, C.D.; Pérez-Huerta, A.; Milazzo, M.; Hall-Spencer, J.M. Effects of ocean acidification on the shells of four Mediterranean gastropod species near a CO_2 seep. *Mar. Pollut. Bull.* **2017**, *124*, 917–928. [CrossRef] [PubMed]
12. Gazeau, F.; Parker, L.M.; Comeau, S.; Gattuso, J.-P.; O'Connor, W.A.; Martin, S.; Pörtner, H.-O.; Ross, P.M. Impacts of ocean acidification on marine shelled molluscs. *Mar. Biol.* **2013**, *160*, 2207–2245. [CrossRef]
13. Hall-Spencer, J.M.; Rodolfo-Metalpa, R.; Martin, S.; Ransome, E.; Fine, M.; Turner, S.M.; Rowley, S.J.; Tedesco, D.; Buia, M. Volcanic carbon dioxide vents show ecosystem effects of ocean acidification. *Nature* **2008**, *454*, 96–99. [CrossRef]

14. Melatunan, S.; Calosi, P.; Rundle, S.D.; Widdicombe, S.; Moody, A.J. Effects of ocean acidification and elevated temperature on shell plasticity and its energetic basis in an intertidal gastropod. *Mar. Ecol. Prog. Ser.* **2013**, *472*, 155–168. [CrossRef]
15. Leung, J.Y.S.; Zhang, S.; Connell, S.D. Is ocean acidification really a threat to marine calcifiers? A systematic review and meta-analysis of 980+ studies spanning two decades. *Small* **2022**, *18*, e2107407. [CrossRef] [PubMed]
16. Barclay, K.M.; Sinclair, C.R.; Leighton, L.R. Patterns of prey selection by the crab *Cancer productus* among three similar gastropod species (*Nucella* spp.). *J. Exp. Mar. Biol. Ecol.* **2020**, *530–531*, 151443. [CrossRef]
17. Parker, L.M.; Ross, P.M.; O'Connor, W.A.; Pörtner, H.O.; Scanes, E.; Wright, J.M. Predicting the response of molluscs to the impact of ocean acidification. *Biology* **2013**, *2*, 651–692. [CrossRef] [PubMed]
18. Boulding, E.G.; Holst, M.; Pilon, V. Changes in selection on gastropod shell size and thickness with wave exposure on northeastern Pacific shores. *J. Exp. Mar. Biol. Ecol.* **1999**, *232*, 217–239. [CrossRef]
19. Brookes, J.I.; Rochette, R. Mechanism of a plastic phenotypic response: Predator-induced shell thickening in the intertidal gastropod *Littorina obtusata*. *J. Evol. Biol.* **2007**, *20*, 1015–1027. [CrossRef]
20. Leung, J.Y.; Connell, S.D.; Nagelkerken, I.; Russell, B.D. Impacts of near-future ocean acidification and warming on the shell mechanical and geochemical properties of gastropods from intertidal to subtidal zones. *Environ. Sci. Technol.* **2017**, *51*, 12097–12103. [CrossRef]
21. Viotti, S.; Sangil, C.; Hernández, C.A.; Hernández, J.C. Effects of long-term exposure to reduced pH conditions on the shell and survival of an intertidal gastropod. *Mar. Environ. Res.* **2019**, *152*, 104789. [CrossRef] [PubMed]
22. Mustapha, N.; Marshall, D.J. Tracking coastal acidification from erosion of gastropod shells: Spatial sensitivity and organism size effect. *Environ. Monit. Assess.* **2021**, *193*, 690. [CrossRef] [PubMed]
23. Mayk, D.; Peck, L.S.; Backeljau, T.; Harper, E.M. Shell thickness of *Nucella lapillus* in the North Sea increased over the last 130 years despite ocean acidification. *Commun. Earth Environ.* **2022**, *3*, 158. [CrossRef]
24. Marshall, D.J.; Tsikouras, B. Compensatory shell thickening in corrosive environments varies between related rocky-shore and estuarine gastropods. *Mar. Environ. Res.* **2024**, *198*, 106536. [CrossRef] [PubMed]
25. Marshall, D.J.; Rashid, A. Organismal responses to coastal acidification informed by interrelating erosion, roundness and growth of gastropod shells. *Zool. Stud.* **2023**, *62*, 41. [CrossRef]
26. Hu, X.; Cai, W.J. Estuarine acidification and minimum buffer zone—A conceptual study. *Geophys. Res. Lett.* **2013**, *40*, 5176–5181. [CrossRef]
27. Checa, A.G.; Macías-Sánchez, E.; Harper, E.M.; Cartwright, J.H.E. Organic membranes determine the pattern of the columnar prismatic layer of mollusc shells. *Proc. R. Soc. B Biol. Sci.* **2016**, *283*, 20160032. [CrossRef]
28. Chadwick, M.; Harper, E.M.; Lemasson, A.; Spicer, J.I.; Peck, L.S. Quantifying susceptibility of marine invertebrate biocomposites to dissolution in reduced pH. *R. Soc. Open Sci.* **2019**, *6*, 190252. [CrossRef]
29. Barclay, K.M.; Gingras, M.K.; Packer, S.T.; Leighton, L.R. The role of gastropod shell composition and microstructure in resisting dissolution caused by ocean acidification. *Mar. Environ. Res.* **2020**, *162*, 105105. [CrossRef]
30. Saley, A.M.; Ninokawa, A.T.; Doan, A.; Gaylord, B. Mussel periostracum protects against shell dissolution. *PLoS ONE* **2025**, *20*, e0327170. [CrossRef]
31. Marin, F.; Luquet, G. Molluscan shell proteins. *Comptes Rendus Palevol* **2004**, *3*, 469–492. [CrossRef]
32. Falini, G.; Albeck, S.; Weiner, S.; Addadi, L. Control of aragonite or calcite polymorphism by mollusk shell macromolecules. *Science* **1996**, *271*, 67–69. [CrossRef]
33. Leung, J.Y.S.; Chen, Y.; Nagelkerken, I.; Zhang, S.; Xie, Z.; Connell, S.D. Calcifiers can adjust shell building at the nanoscale to resist ocean acidification. *Small* **2020**, *16*, 2003186. [CrossRef]
34. Carlson, R.R.; Lewis, M.A.; Ninokawa, A.T.; Saley, A.M.; Hill, T.M.; Gaylord, B. Shell dissolution rates differ fourfold between mussel species. *R. Soc. Open Sci.* **2025**, *12*, 250664. [CrossRef]
35. Peck, V.L.; Tarling, G.A.; Manno, C.; Harper, E.M. Outer organic layer and internal repair mechanism protects pteropod *Limacina helicina* from ocean acidification. *Deep Sea Res. Part II* **2016**, *127*, 41–52. [CrossRef]
36. Marshall, D.J.; Tsikouras, B. Clay-shielded estuarine gastropods are better protected against environmental acidification than unshielded individuals. *Sci. Total Environ.* **2023**, *866*, 161367. [CrossRef]
37. Waldbusser, G.G.; Steenson, R.A.; Green, M.A. Oyster shell dissolution rates in estuarine waters: Effects of pH and shell legacy. *J. Shellfish Res.* **2011**, *30*, 659–669. [CrossRef]
38. Lee, H.C.; Glasby, C.J.; Schulze, A.; Raven, H.; Tan, S.K.; Arai, T.; Jin, A.M.; Tal'ah, N.N.; Zarifi, A.; Marshall, D.J. Dramatic enhancement of macrozoobenthic species β-diversity in response to artificial breakwater construction along a tropical coastline. *Diversity* **2024**, *16*, 742. [CrossRef]
39. Cui, Z.; Hu, L.; Li, C.; Zhang, Z.; Guo, X.; Wang, H. Identification of *Saccostrea mordax* and a new species *Saccostrea mordoides* sp. nov. (Bivalvia: Ostreidae) from China. *J. Shellfish Res.* **2021**, *40*, 63–75. [CrossRef]

40. Lukehurst, S.S.; Tan, S.K.; Tan, K.S.; Dehm, J.; Hewavitharane, C.; Wells, F.E. Clarifying the identities of *Saccostrea scyphophilla* (Péron & Lesueur, 1807) and *S. mordax* (Gould, 1850) (Bivalvia: Ostreidae) from the Indo-Pacific. *Zootaxa* **2026**, *5799*, 001–031. [CrossRef]
41. Bednaršek, N.; Tarling, G.A.; Bakker, D.C.E.; Fielding, S.; Feely, R.A. Dissolution dominating calcification process in polar pteropods close to the point of aragonite undersaturation. *PLoS ONE* **2014**, *9*, e109183. [CrossRef] [PubMed]
42. Langer, G.; Nehrke, G.; Baggini, C.; Rodolfo-Metalpa, R.; Hall-Spencer, J.M.; Bijma, J. Limpet ocean acidification-induced shell corrosion by thickening of aragonitic shell layers. *Biogeosciences* **2014**, *11*, 7363–7368. [CrossRef]
43. Peck, V.L.; Oakes, R.L.; Harper, E.M.; Manno, C.; Tarling, G.A. Pteropods counter mechanical damage and dissolution through extensive shell repair. *Nat. Commun.* **2018**, *9*, 264. [CrossRef]
44. Marshall, D.J.; McQuaid, C.D.; Williams, G.A. Non-climatic thermal adaptation: Implications for species' responses to climate warming. *Biol. Lett.* **2010**, *6*, 669–673. [CrossRef] [PubMed]
45. Abdelwahab, A.; Abas, P.E.; Marshall, D.J.; Schirmer, M.; Azffri, S.L.; Gödeke, S. Hydrogeochemistry of submarine groundwater discharge along a Bruneian coastline: Iron and aluminum enrichment along with coastal acidification. *Environ. Earth Sci.* **2025**, *85*, 15. [CrossRef]
46. Proum, S.; Santos, J.H.; Lim, L.-H.; Marshall, D.J. Tidal and seasonal variation in carbonate chemistry, pH and salinity for a mineral-acidified tropical estuarine system. *Reg. Stud. Mar. Sci.* **2018**, *17*, 17–27. [CrossRef]
47. Barillé, L.; Le Bris, A.; Méléder, V.; Launeau, P.; Robin, M.; Louvrou, I.; Ribeiro, L. Photosynthetic epibionts and endobionts of Pacific oyster shells from oyster reefs in rocky versus mudflat shores. *PLoS ONE* **2017**, *12*, e0185187. [CrossRef]
48. Jesus, B.; Rosa, P.; Mouget, J.-L.; Méléder, V.; Launeau, P.; Barillé, L. Spectral-radiometric analysis of taxonomically mixed microphytobenthic biofilms. *Remote Sens. Environ.* **2014**, *140*, 196–205. [CrossRef]
49. Marshall, D.J.; Baharuddin, N.; McQuaid, C.D. Behaviour moderates climate warming vulnerability in high-rocky-shore snails: Interactions of habitat use, energy consumption and environmental temperature. *Mar. Biol.* **2013**, *160*, 2525–2530. [CrossRef]
50. Marshall, D.J.; Dong, Y.; McQuaid, C.D.; Williams, G.A. Thermal adaptation in the intertidal snail *Echinolittorina malaccana* contradicts current theory by revealing the crucial roles of resting metabolism. *J. Exp. Biol.* **2011**, *214*, 3649–3657. [CrossRef] [PubMed]
51. Taylor, J.D.; Kennedy, W.J. The influence of the periostracum on the shell structure of bivalve molluscs. *Calcif. Tissue Int.* **1969**, *3*, 274–283. [CrossRef] [PubMed]
52. Taylor, J.D. Field observations of prey selection by the muricid gastropods *Thais clavigera* and *Morula musiva* feeding upon the intertidal oyster *Saccostrea cucullata*. In *The Marine Flora and Fauna of Hong Kong and Southern China II*; Morton, B., Ed.; Hong Kong University Press: Hong Kong, China, 1990; pp. 836–855.
53. Zardi, G.I.; Monsinjon, J.; McQuaid, C.D.; Seuront, L.; Orostica, M.; Want, A.; Firth, L.B.; Nicastro, K.R. Foul-weather friends: Modelling thermal stress mitigation by symbiotic endolithic microbes in a changing environment. *Glob. Change Biol.* **2021**, *27*, 2549–2560. [CrossRef]
54. Naviaux, J.D.; Subhas, A.V.; Rollins, N.E.; Dong, S.; Berelson, W.M.; Adkins, J.F. Temperature dependence of calcite dissolution kinetics in seawater. *Geochim. Cosmochim. Acta* **2019**, *246*, 363–384. [CrossRef]
55. Coleman, D.; Byrne, M.; Davis, A. Molluscs on acid: Gastropod shell repair and strength in acidifying oceans. *Mar. Ecol. Prog. Ser.* **2014**, *509*, 203–211. [CrossRef]
56. Leung, J.Y.S.; Russell, B.D.; Connell, S.D. Mineralogical plasticity acts as a compensatory mechanism to the impacts of ocean acidification. *Environ. Sci. Technol.* **2017**, *51*, 2652–2659. [CrossRef] [PubMed]

Disclaimer/Publisher's Note: The statements, opinions and data contained in all publications are solely those of the individual author(s) and contributor(s) and not of MDPI and/or the editor(s). MDPI and/or the editor(s) disclaim responsibility for any injury to people or property resulting from any ideas, methods, instructions or products referred to in the content.